

Experimental and Theoretical Studies of 1-vinyl-3-hexylimidazolium Iodide ([VHIM]I) as Corrosion Inhibitor for the Mild Steel in Sulfuric Acid Solution

Li Feng¹, Shengtao Zhang^{1,3,*}, Song Yan², Shenyong Xu¹, Shijin Chen⁴

¹ School of Chemistry and Chemical Engineering, Chongqing University, Chongqing 400044, P.R. China.

² National Engineering Laboratory for Pipeline Safety, China University of Petroleum, Beijing 102249, P.R. China.

³ Material Corrosion and Protection Key Laboratory of Sichuan Province, Zigong 643000, P.R. China.

⁴ Bomin electronics Ltd, Meizhou 514021, P.R. China.

*E-mail: stzhang_cqu@163.com

Received: 10 December 2016 / Accepted: 12 January 2017 / Published: 12 February 2017

In order to explore the corrosion inhibition mechanism of 1-vinyl-3-hexylimidazolium iodide with different concentration for mild steel in 0.5M H₂SO₄ at 298K, experimental and theoretical studies were carried out. Not only weight loss but also electrochemical experiments reveal that 1-vinyl-3-hexylimidazolium iodide ([VHIM]I) has higher inhibition efficiency. And all experiments have good consistency. The inhibition efficiency was more than 96% comparing with the blank when the concentration was 5mM. It indicates that [VHIM]I adsorbed on the surface of invested metal by forming a film to protect metal. In addition, SEM observation and ATR-IR spectra was used to further confirmed the above. The Langmuir adsorption isotherm was the most proper adsorption model for the adsorption of [VHIM]I molecule on mild steel surface. Moreover, theoretical calculation and molecular dynamic (MD) simulation also manifest that [VHIM]I was absorbed mightily on the metal surface in a parallel mode.

Keywords: corrosion, inhibitor, mild steel, Electrochemical experiments, molecular dynamic simulation, sulfuric acid solution.

1. INTRODUCTION

Because of its exceptional mechanical properties, the mild steel is widely used in many industries such as transportation industry, machinery manufacturing, bridge construction, and marine industry [1]. However, its corrosion causes economic and energy losses all over the world, implying

that using an inhibitor to prevent this valuable metal corrosion is necessary in the future [2-4]. In the chemical and oil industry especially in acidic media, the first line of defense against corrosion is adding of inhibitors [5, 6]. The typical inhibitors are organic matters, which include the heteroatoms, for instance, nitrogen, oxygen, phosphorous and sulphur, generally exhibiting the best protection for the metal [5-8]. According to a lot of data, most of the organic inhibitors were adsorbed on metal by displacing water molecules to forming a compact barrier film [8-14].

However, there are several disadvantages produced from application of organic inhibitors such as toxicity, environmental pollution, low thermal stability and so on. Therefore, a great urgency of developing green environment-friendly corrosion inhibitors has potential significant meaning [15]. Up to now, many kinds of functional groups have been introduced as inhibitors [16-17]. And some ionic liquids imidazolium compounds have been applied to prevent copper, steel and aluminum corrosion from corrosive environment due to their tempting properties such as high ionic conductivity, excellent thermal stability, non-toxicity, large electrochemical windows [18-32]. Because they have the -C=N- group and electric negative nitrogen in these studied molecule, there is excellent inhibition efficiency by forming the inhibitory film on the metal surface. Perhaps there is a synergistic effect between the imidazole and iodine ion for 1-vinyl-3-hexylimidazolium iodide [19, 33].

For this study, the purpose is to investigate the corrosion inhibition effect of Iodide imidazole-based ionic liquid compound, namely the 1-vinyl-3-hexylimidazolium iodide ([VHIM]I), on the inhibition of mild steel in 0.5 M sulfuric acid solution at 298K. For the mild steel inhibition, the inhibitive performance of the inhibitor was explored by the electrochemical methods containing potentiodynamic polarization experiments and electrochemical impedance spectroscopy (EIS), weight loss, FESEM techniques and ATR-FTIR spectra in 0.5M H₂SO₄ solution at 298K. The protective effect of [VHIM]I for mild steel was explained by the quantum chemical calculations. Moreover, the inhibition mechanism is further studied by the molecular dynamic (MD) simulation to interpret the inhibition effects of 1-vinyl-3-hexylimidazolium iodide ([VHIM]I) for the mild steel. Hence, the inhibitive mechanism of studied inhibitor is explained concretely based on experiment and theoretical calculation.

2. MATERIALS AND PREPARATIONS

2.1 Materials

The components (wt. %) of mild steel are 0.05% C, 1.54% Mn, 0.19% Si, 0.23% Cu, 0.19% Mo, 0.2% Ni, 0.2% Cr, and the rest is iron. For each experiment, sulfuric acid solution (H₂SO₄, Aladdin, 99.9%), [VHIM]I (Shanghai Cheng Jie Chemical Co. LTD, 99%) (Fig. 1) and absolute ethanol (C₂H₅OH, Aladdin, 99.9%) were used without any purification. The CHI 660C electrochemical workstation (Shanghai Chenhua CO, LTD) was employed for electrochemical experiments. In addition, the mild steel specimens with dimensions of 1.00 cm × 1.00 cm × 1.00 cm for electrochemical experiments, which were embedded in epoxy resin first then mounted in Teflon. While weight loss tests used the dimensions of specimen were 3.00 cm × 2.00 cm × 1.00 cm, differently.

The blank solution is 0.5 M H₂SO₄ solution without any inhibitors and the test solution is prepared by adding corresponding concentration [VHIM]I in the blank solution (0.1, 0.5, 1.0, 2.0, 5.0 mM). Before each experiment, steel specimens were polished by abrasive papers (400, 800, 1200, 2000 grit) in the first place, then washed with distilled water and anhydrous ethanol ultrasonically, finally dried at room temperature. The temperature of 298 K was controlled using aqueous thermostat.

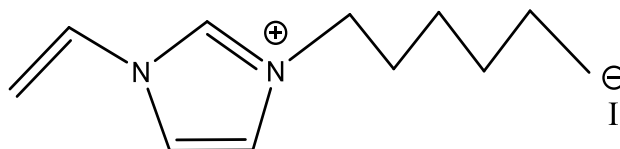


Figure 1. The chemical structure of 1-vinyl-3-hexylimidazolium iodide ([VHIM]I).

2.2 Electrochemical experiments

Applying a typical three-electrode cell system to proceed the potentiodynamic experiments and EIS measurements at 298K. Here, working electrode (WE) is the specimen assembled with the mild steel, reference electrode is saturated calomel electrode (SCE) and the counter electrode is platinum electrode (CE). Prior to electrochemical tests, the electrode was immersed in the test solution for 1000 seconds in order to reach a stable state. About electrochemical impedance spectroscopy (EIS) measurements, the range of frequency is 100 kHz to 10 m Hz and the excitation signal amplitude is 5mV at the OCP. Then, the relevant parameters were obtained and analyzed by Zsimpwin software. For potentiodynamics experiments, the potential range is ± 250 mV based on the OCP and scan rate is 2 mVs⁻¹. Moreover, the Tafel data were obtained from Tafel region with extrapolation method. All experiments were conducted five times to get the experimental reproducibility.

2.3 Weight loss measurements

The mild steel specimens were weighted and suspended in the blank solution and in the presence of 1-vinyl-3-hexylimidazolium iodide ([VHIM]I) at corresponding concentrations (0.1, 0.5, 1.0, 2.0, 5.0 mM) for 4 hours at 298K. Whereafter, the specimens were descaled by the rust removal solution (Zn powders and 20% NaOH), then degreased with anhydrous ethanol and dried at room temperature. At last, the specimens were weighted again accurately in order to get corrosion rates and inhibition efficiency.

2.4 Surface characterization

Prior to tests, samples were prepared as described above. After being immersed in 0.5M H₂SO₄ and in presence of 5 mM 1-vinyl-3-hexylimidazolium iodide ([VHIM]I) for 4 hours at 298 K. The surface morphology of the samples were detected and compared by scanning electron microscopy

(SEM, JEOL-JSM-7800F-Japan). The accelerating voltage is 15 kV.

2.5 ATR-IR spectra experiments

The Fourier transform infrared (ATR-IR) spectras were obtained on the steel surface using ATR-IR spectrometer (BRUKER, Germany) in reflection mode. Samples were immersed in 5mM 1-vinyl-3-hexylimidazolium iodide ([VHIM]I) solution for 4 hours, degreased with Anhydrous ethanol and dried at 298K before testing. At the same time, pure substance was also tested with KBr for comparison. The range of FT-IR spectra wavenumber is 500-4000 cm^{-1} and the spectral resolution is 2 cm^{-1} .

2.6 Calculation methods

The Gaussian 09W software was used to do the Quantum chemical calculation. The B3LYP functional with 6311++G (d, p) basis set was used to geometrically optimized the molecular structure of 1-vinyl-3-hexylimidazolium iodide ([VHIM]I) by density functional theory (DFT). The energy of lowest unoccupied molecular orbital (E_{LUMO}), the energy of highest occupied molecular orbital (E_{HOMO}), energy gap ($\Delta E = E_{\text{LUMO}} - E_{\text{HOMO}}$), and dipole moment (μ) were obtained from Quantum chemical calculation.

Moreover, the molecular dynamic (MD) simulation was conducted in aqueous phase (Material Studio 7.0, Accelrys Inc).The adsorption process was researched between [VHIM]I and the Fe (110) surface by with 298 K, NVT ensemble, a time step of 1 fs and simulation time of 1000 ps. At the same time, the corresponding parameters were received, the E_{Total} is the energy of the copper crystal together with the adsorbed inhibitor molecule, E_{Fe} is the energy of the Fe crystal, $E_{\text{Inhibitor}}$ is the energy of the inhibitor molecular and $E_{\text{Fe-inhibitor}}$ is the binding energy.

3. RESULTS AND DISCUSSION

3.1 polarization measurements

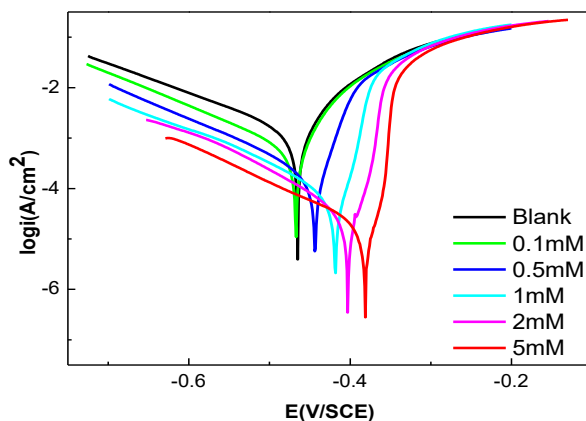


Figure 2. Polarization curves for mild steel in the presence of 1-vinyl-3-hexylimidazolium iodide ([VHIM]I) and the blank at 298K.

Table 1. Polarization relevant parameters for the mild steel in the presence of [VHIM]I at 298 K.

<i>C</i> (mM)	<i>E_{corr}</i> (V/SCE)	<i>I_{corr}</i> (mA cm ⁻²)	β_c (mV s ⁻¹)	β_a (mV s ⁻¹)	η (%)
Blank	-0.475	1.840	168.4	101.6	—
0.1	-0.477	1.010	147.4	102.1	45.1
0.5	-0.449	0.340	136.4	113.4	81.5
1.0	-0.449	0.136	127.4	120.8	92.6
2.0	-0.403	0.060	113.9	119.2	96.7
5.0	-0.379	0.042	143.2	139.0	97.7

The potentiodynamic polarization plots for mild steel in 0.5M H₂SO₄ solution at 298K with different concentration of 1-vinyl-3-hexylimidazolium iodide ([VHIM]I) were showed as Fig. 2. The relevant parameters, the corrosion potential (*E_{corr}*), corrosion current density (*I_{corr}*), anodic and cathodic Tafel slope (β_c , β_a), and the inhibition efficiency (η) were obtained and listed in Table 1.

The inhibition efficiency (η %) of [VHIM]I can be obtained by the following (1) [34-39]:

$$\eta = \left(1 - \frac{I_{corr}}{I_{corr,0}}\right) \times 100\% \quad (1)$$

Where *I_{corr,0}* and *I_{corr}* are the corrosion current densities without and with [VHIM]I.

It can be seen from Fig. 2 that *E_{corr}* moved to the positive direction and *I_{corr}* decreased obviously comparing with the blank as the increase of corrosion inhibitor concentration. That is to say, the addition of inhibitor concentration can prevent the corrosion of the mild steel more effectively [40-42]. Obviously, the [VHIM]I is a high-efficiency inhibitor comparing with previous related reports [34, 43]. In addition, β_a and β_c values have no significant change with the increase of [VHIM]I, indicating that the inhibition mechanism does not change in the presence of [VHIM]I in 0.5M H₂SO₄ solution [19, 34]. As the increase of inhibitor concentration, the values of η (%) increased and the maximum value reached to 97.7%. It was surprising that the inhibition efficiency was already more than 92.6% at 1Mm which is much better than some reports [39, 43, 44]. These results imply that the corrosion of steel is inhibited on account of forming a protective film on metal surface [34-39]. Here, negatively charged iodine ions were adsorbed up first, then midazole-base ions were absorbed easily [45]. At the same time, [VHIM]I occupied active sites of mild steel by adsorbing on the surface, the corrosion was decreased.

3.2 Electrochemical impedance spectroscopy (EIS)

The Nyquist curves of this study were showed in Fig. 3. The EIS data was simulated to fit the equivalent circuit (Fig. 4) using ZSimpwin software. And the related data was showed in Table 2. The equivalent circuit contains some electrochemical parameters. Where *R_s* is the solution resistance, CPE is constant phase element, *R_{ct}* represents the charge transfer resistance, inductive elements are L and *R_L*. The CPE is described by the following [34, 39, 43]:

$$Z_{CPE} = \frac{1}{Y(j\omega)^n} \quad (2)$$

Here, Y_0 is the CPE constant, j is the imaginary root w is the angular frequency, and n is the deviation parameter. Therefore, the C_{dl} is calculated according to the following [19, 34, 39]:

$$C_{dl} = Y(w)^{n-1} = Y(2\pi f z_{im-Max})^{n-1} \tag{3}$$

The η (%) values are calculated as follows [19, 34, 39]:

$$\eta = \frac{R_{ct} - R_{ct,0}}{R_{ct}} \times 100\% \tag{4}$$

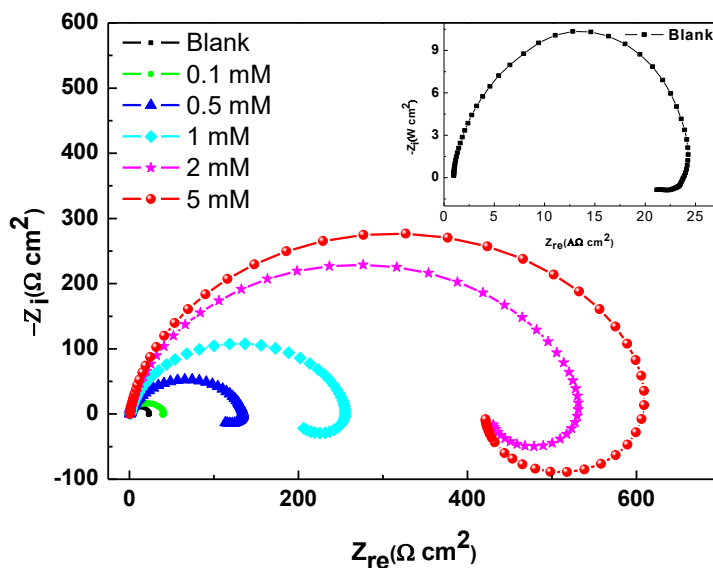


Figure 3. Nyquist impedance plots for the mild steel in the absence and presence of [VHIM]I in 0.5M H_2SO_4 solution at 298K.

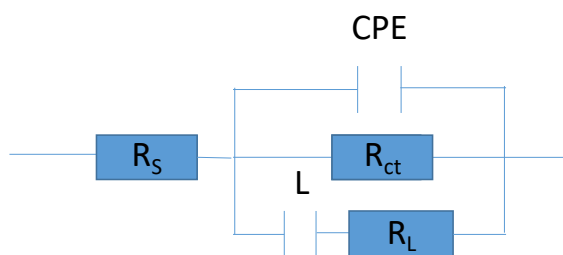


Figure 4. The equivalent circuits with inductive loop used for fitting the EIS experimental data.

Table 2. Impedance relevant parameters of mild steel for this study.

C (mM)	R (cm ²)	$Y_0 \times 10^{-5}$ (Ω cm ²)	n	C_{dl} (μFcm ⁻²)	R_{ct} (Ω cm ²)	L (Ω cm ²)	R_L (Ω cm ²)	η (%)
blank	0.93	17.75	0.90	82.1	23.7	70.6	181	—
0.1	0.92	20.06	0.86	66.9	40.9	199.3	571	42.1
0.5	0.89	17.21	0.84	50.7	134.9	4835	471	82.4
1	0.65	7.956	0.89	30.0	258.4	2355	810	90.8
2	0.66	5.292	0.89	21.5	541.2	4430	2029	95.6
5	0.78	4.057	0.92	20.6	628.3	1266	1271	96.2

It is observed from Fig. 3 that Nyquist plots have two parts at a low concentration and at the blank while have only one part at a high concentration. When the concentration is low, the Nyquist curves contain a depressed capacitive loop at high frequency and an inductive loop at low frequency. The depressed capacitive loop is related to the time constant of charge transfer and double layer behavior, but the inductive loop is related to the relaxation process of adsorbed species such as re-dissolution of the working electrode surface or (SO_4^{2-}) ads, (H^+) ads and so on [37, 39]. The heterogeneousness and rough electrode surface make the capacitive loop present depressed semicircle [36-39]. This phenomenon is caused by frequency dispersion [39]. It also shown that the capacitive loop diameters increase with the incremental [VHIM]I concentration. They are markedly larger comparing with the blank. It indicates that the main controlled factor of corrosion process is the charge transfer process, so the steel corrosion is impeded as the addition of [VHIM]I by adsorption [43]. Moreover, the shape of the Nyquist plots with different concentration of [VHIM]I is similar, indicating that the corrosion mechanism has not changed [19].

According to the Table 2, the R_L , L and R_{ct} values increase distinctly as increasing inhibitor concentration, while the values of C_{dl} and Y_0 decrease comparing with the blank. This suggests that [VHIM]I molecules replaced water molecules on the metal surface, which causes lower local dielectric constant, smaller electrode surface area, and thicker electric double-layer [37-39]. In addition, the values of η (%) raise with the addition of [VHIM]I concentration and the best inhibition efficiency is up to 96.2% at 5mM. Thus, the mild steel was protected efficiently on account of forming a dense layer of protective film.

3.3 Weight loss measurement

Table 3. The results of weight loss measurements for mid steel in 0.5M H_2SO_4 solution with different concentration of [VHIM]I at 298K.

C(mM)	ν ($\text{m}^{-1}\text{h}^{-1}$)	η (%)	θ
Blank	17.7614	—	—
0.1	10.7273	39.6	0.3960
0.5	5.1545	71.0	0.7098
1.0	2.4432	86.2	0.8624
2.0	1.4773	94.6	0.9458
5.0	0.4636	97.4	0.9739

The relevant parameters of weight loss measurement were calculated and listed in Table 3. There are corrosion rate (ν), inhibition efficiency (η %) and surface coverage (θ) of [VHIM]I obtained by the following equations [40]:

$$\nu = \frac{W}{St} \quad (5)$$

$$\eta = \frac{\nu_0 - \nu}{\nu_0} \times 100\% \quad (6)$$

$$\theta = \frac{v_0 - v}{v_0} \quad (7)$$

Where w is the weight loss of the sample, S is the total surface area of the sample, and t is the immersion time. The v_0 and v are the corrosion rates of specimens with different concentration of [VHIM]I.

From Table 3, it is obvious that the corrosion rate lowered sharply as the increase of inhibitor concentration. This phenomenon manifests that the [VHIM]I can prevent the metal corrosion in corrosion media at 298K by forming a compact film on the metal surface [34]. The inhibition efficiency (η) is well consistent with this phenomenon.

3.4 ATR-FTIR spectra

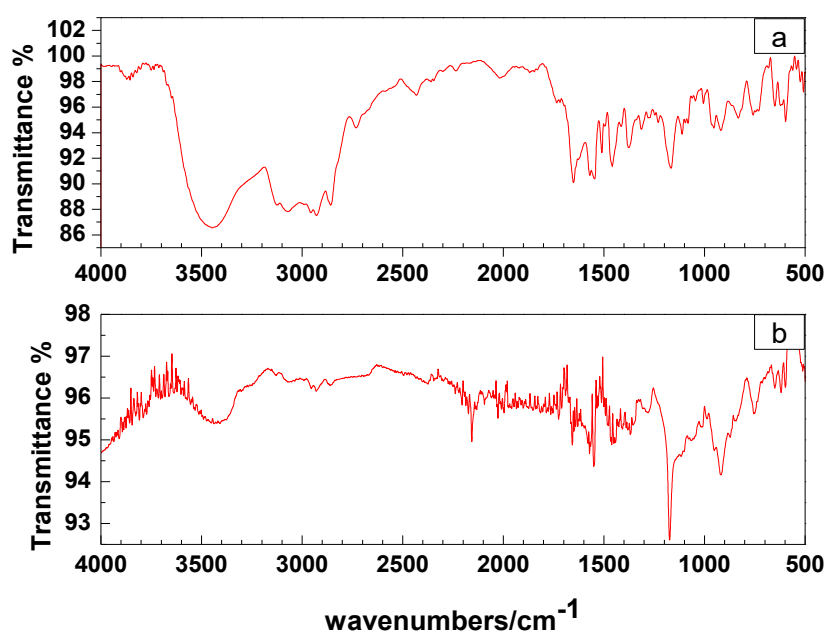


Figure 5. ATR-IR spectra of [VHIM]I (a) and the [VHIM]I film on the mild steel (b).

ATR-IR spectras of [VHIM]I (a) and the [VHIM]I film on the metal surface (b) were showed in Fig. 5. It can be used to analyze the interaction of inhibitor on metal surface. In Fig. 5 (a) the bands at 1651 cm^{-1} and 1509 cm^{-1} were corresponding to the $\text{C}=\text{N}$, while in Fig. 5 (b) the band at 1509 cm^{-1} disappeared [46]. Besides, in Fig 5 (a) the band at 1166 cm^{-1} was corresponding to the $\text{C}-\text{N}$, but in Fig. 5 (b) this band shifted from 1166 cm^{-1} to 1173 cm^{-1} . These results suggest that the inhibitor moleculars with the N atoms are absorbed to the mild steel surface by chemical bonds [47].

3.5 Adsorption isotherm

There are various adsorption isotherms, Langmuir, Frumkin, Temkin, and Bockris-Swinkel isotherms, which were used to fit the experimental data from the weight loss measurements [43].

Obviously, the Langmuir isotherm (eq. (6)) adsorption is the most suitable, the mode is monolayer adsorption, the R^2 is up to 0.9997 (Fig. 6). The relevant parameters including the adsorption equilibrium constant of inhibitor (K_{ads}) and the standard free energy of adsorption process (ΔG_{ads}) were calculated according to the following [41]:

$$\frac{C}{\theta} = \frac{1}{K_{ads}} + C \quad (8)$$

$$K_{ads} = \frac{1}{55.5} \exp\left(\frac{-\Delta G_{ads}}{RT}\right) \quad (9)$$

Here, containing the degree of the coverage (θ), the concentration of [VHIM]I (C), and the absolute temperature (T).

Due to the negative ΔG_{ads} values the adsorption of [VHIM]I on metal surface is regarded as a spontaneous process [47]. Generally, when the value of ΔG_{ads} is higher than -20 kJmol^{-1} , the adsorption is mainly physical adsorption on account of electrostatic interaction between the metal and inhibitor molecules. While the adsorption is considered involving chemical adsorption because the ΔG_{ads} values are around or less than -40 kJ mol^{-1} , which is related to the new chemical bond [34-39, 47]. Here, the value of ΔG_{ads} is $-31.48 \text{ kJmol}^{-1}$, so the adsorption of [VHIM]I on metal surface is regarded including chemical adsorption and physical adsorption.

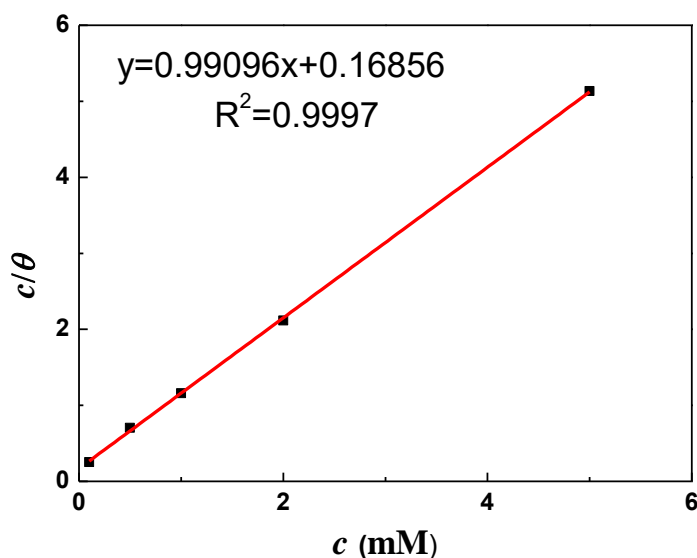


Figure 6. Langmuir adsorption isotherm of [VHIM]I on mild steel surface in 0.5 M H_2SO_4 solution at 298 K.

3.6 Morphological analysis

The SEM micrographs of mild steel specimens polished freshly (a), immersed in the blank (b) and immersed in 5 mM [VHIM]I (c) for 4 hours at 298 K were shown in Fig. 6. It can be seen the steel morphology is smooth (Fig. 7 (a)) before being immersed.

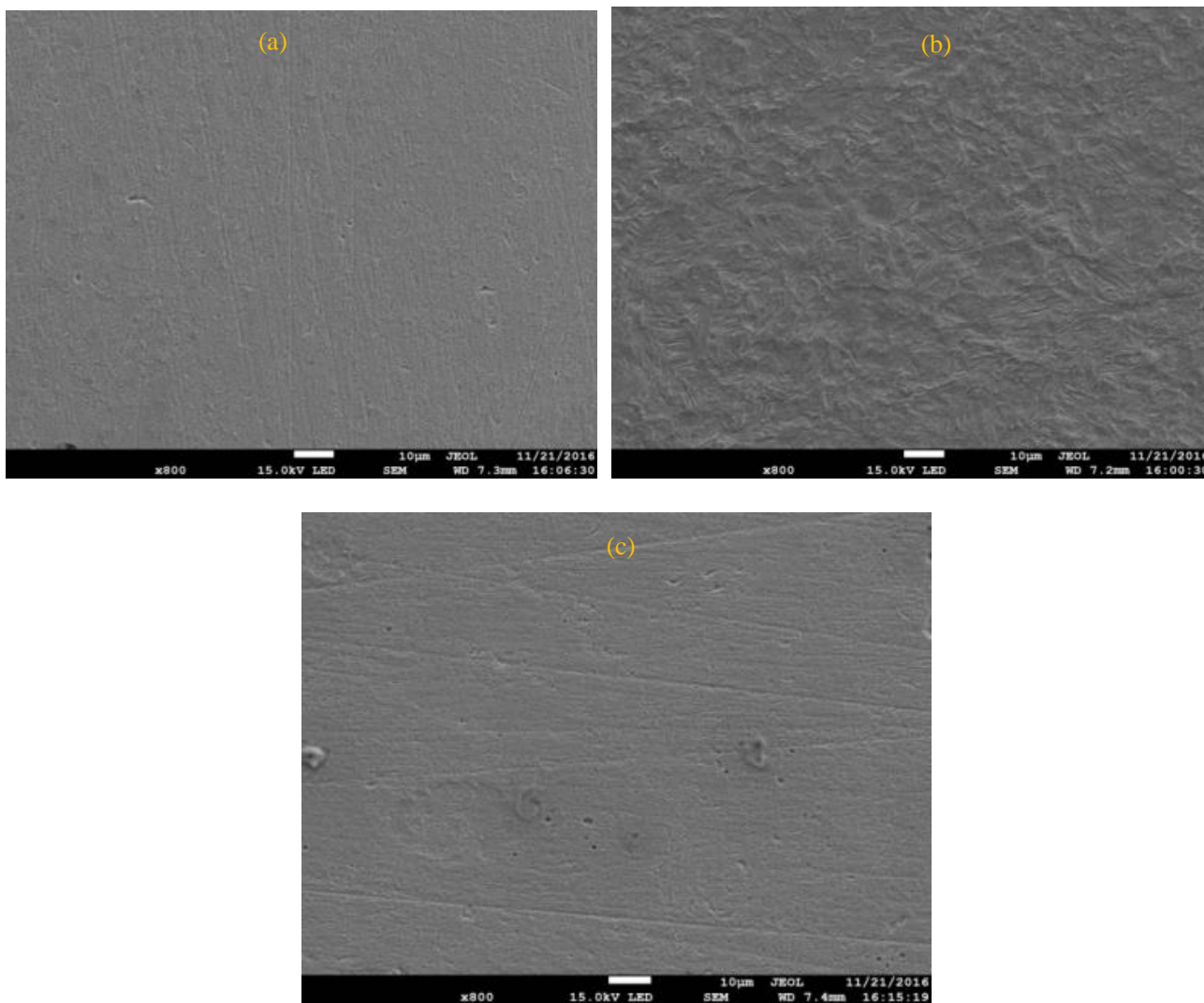
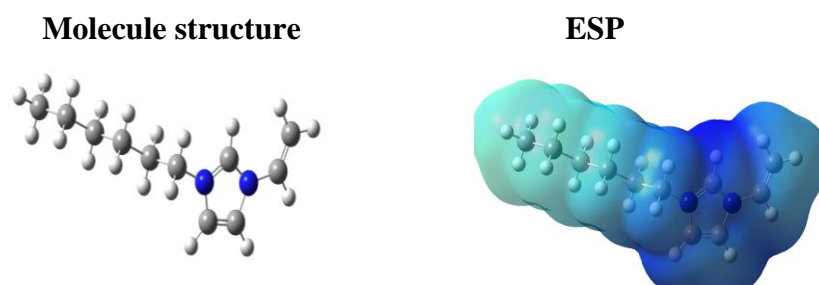


Figure 7. SEM morphology of the mild steel specimen at 298K.

While the sample (Fig. 7 (b)) is corroded seriously after being immersed in the corrosive medium. Nevertheless, the steel sample (Fig. 7 (c)) is more smooth in the presence of [VHIM]I than one in the blank. It demonstrates that [VHIM]I can effectively inhibit the corrosion process for invested metal in 0.5 M H₂SO₄ media at 298 K.

3.7 Theoretical calculation



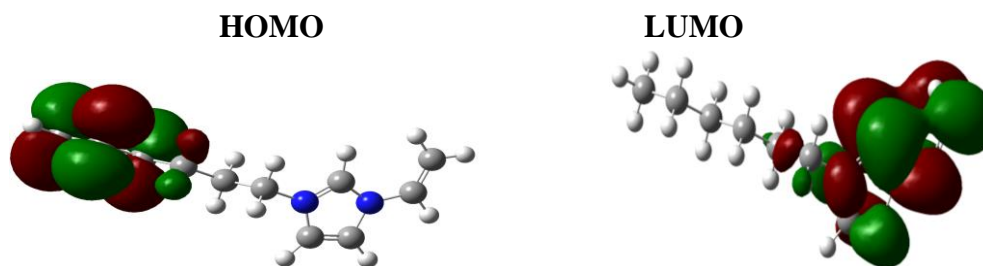


Figure 8. Optimized geometric structures, Electrostatic surface potential and frontier molecular orbital of [VHIM]I.

Table 4. The parameters about Quantum chemical calculation.

E_{HOMO} (eV)	E_{LUMO} (eV)	ΔE (eV)	μ (Debye)
-0.41297	-0.21200	0.20097	8.9196

Quantum chemical calculations have been conducted in order to understand inhibition mechanism of [VHIM]I for mild steel in corrosion media at 298K. Especially, optimized geometric structures, Electrostatic surface potential and frontier molecular orbital of [VHIM]I including the electron density distributions of HOMO and LUMO for [VHIM]I were shown as Fig. 8. Then, the parameters about quantum chemical calculation were showed in Table 4. There are not only including the energy of the highest occupied molecular orbital (E_{HOMO}) but also containing the lowest unoccupied molecular orbital (E_{LUMO}) of the inhibitor molecular. Besides the energy gap ($\Delta E = E_{\text{LUMO}} - E_{\text{HOMO}}$) and dipole moment (μ) are analyzed.

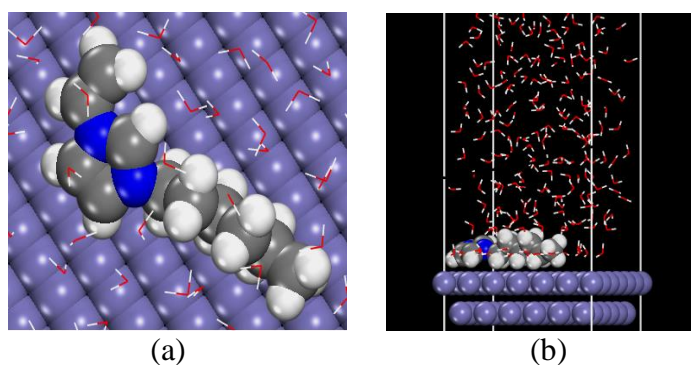


Figure 9. The equilibrium configuration of the molecular dynamics simulation (top view (a), side view (b)).

Obviously, the orbital of LUMO and HOMO occupied the whole inhibitor molecule, which indicates the whole inhibitor molecule can adsorb on metal surface completely. On the basis of the frontier molecular orbital theory, E_{LUMO} is associated with the electronic capabilities of molecules while E_{HOMO} is relevant to the molecular ability of electron donors [39]. The N atoms in imidazole ring

donated the lone pair electrons to the vacant d orbital of Fe, so a protective film was formed by adsorption [39, 46]. Based on the above, metal corrosion was inhibited effectively. From the previous data, the energy gap (ΔE) is generally associated with chemical stability of the molecule [48]. Here, the ΔE value of molecule is lower, so it has higher inhibition efficiency for mild steel corrosion. Besides, the high dipole moment (μ) suggests that the inhibitor molecule is easier to be polarized to interact with metal. This is consistent with the above experimental results.

3.8 Molecular dynamic (MD) simulation

Molecular dynamics simulation was carried out to further study the mechanism of corrosion inhibition in aqueous phase. And the results were showed in Fig. 9 including the top view (a) and the side view (b), which is the equilibrium configuration of the inhibitor adsorbed on the mild steel (110) surface. Obviously, it is a strong absorption of inhibitor on metal surface by a parallel mode from the picture. There was a maximize contact between metal surface and inhibitor molecule, minimize mild steel surface area were corroded in corrosive solution [39]. And it excited a chemical adsorption between inhibitor and the metal surface. Moreover, the value of interaction energy is $-191.225 \text{ kJ mol}^{-1}$, suggesting it was a strong absorption between [VHIM]I and mild steel surface to form a protective film [49]. At the same time, the water molecules of metal surface were replaced by the inhibitors, so the corrosion of the mild steel surface was inhibited efficiently. This result is similar with the results of above mentioned.

4. CONCLUSION

(1) Potentiodynamic polarization curves manifests that inhibition efficiency of [VHIM]I increases as incremental inhibitor concentration.

(2) EIS shows that R_L , L and R_{ct} values increase while Y_0 and C_{dl} decrease as the increase of inhibitor concentration.

(3) The weight loss tests also indicate that the [VHIM]I is excellent inhibitor for invested steel in $0.5\text{M H}_2\text{SO}_4$ at 298K and have good consistency with the results of EIS, polarization curves experiments.

(4) The SEM and ATR-IR spectra show that [VHIM]I perform a chemical adsorption on mild steel surface to inhibit the metal corrosion by occupying the active area on the metal surface.

(5) The Langmuir isotherm model is the most fitful model for this study with spontaneous chemical adsorption and physical adsorption.

(6) Theoretical research proves that the [VHIM]I molecular adsorb to the metal surface by a parallel pattern.

ACKNOWLEDGMENTS

This research was supported by National Natural Science Foundation of China (No. 21376282), Sail plan of Guangdong, China (No. 2015YT02D025), and the Opening Project of Material Corrosion and Protection Key Laboratory of Sichuan Province (No. 2016CL20).

References

1. M. M. Osman and M. N. Shala, *Mater. Chem. Phys.*, 77 (2003) 261.
2. P. C. Okafor, X. Liu and Y. G. Zheng, *Corros. Sci.*, 51 (2009) 761.
3. A. A. Farag and M. A. Hegazy, *Corros. Sci.*, 74 (2013) 168.
4. B.J. Gao, X. Zhang and Y.L. Sheng, *Mater. Chem. Phys.*, 108 (2008) 375.
5. M.A. Amin and M.M. Ibrahim, *Corros. Sci.*, 53 (2011) 873.
6. S. Herrmann, M. Kostrzewa, A. Wierschem and C. Streb, *Angew. Chem. Int. Ed.*, 53 (2014) 13596.
7. K. Stanly Jacob and G. Parameswaran, *Corros. Sci.*, 52 (2010) 224.
8. D.Q. Zhang, L.X. Gao and G.D. Zhou, *Corros. Sci.*, 46 (2004) 3031.
9. M. A. J. Mazumder, H. A. Al-Muallem and S. A. Ali, *Corros. Sci.*, 90 (2015) 54.
10. V. Branzoi, F. Branzoi and M. Baibarac, *Mater. Chem. Phys.*, 65 (2000) 288.
11. M. A. Veloz and I. G. Martínez, *Corrosion*, 62 (2006) 283.
12. Y. Qiang, S. Zhang, S. Xu and L. Yin, *Int. J. Electrochem. Sci.*, 11 (2016) 3147.
13. A. Popova, M. Christov and A. Vasilev, *Corros. Sci.*, 49 (2007) 3290.
14. M. S. Morad, *Corros. Sci.*, 42 (2000) 1307.
15. R. N. Das and K. Roy, *Mol. Diversity*, 17 (2013) 151.
16. G. Kılınçeker and H. Demir, *Anti-Corros. Methods Mater.*, 60 (2013) 134.
17. N.V. Likhanova, M.A. Domínguez-Aguilar, O. Olivares-Xometl, N. Nava-Entzana, E. Arce and H. Dorantes, *Corros. Sci.*, 52 (2010) 2088.
18. X. H. Li, S. D. Deng and H. Fu, *Corros. Sci.*, 53 (2011) 1529.
19. X. W. Zheng, S. T. Zhang, W. P. Li, L. L. Yin, J. H. He and J. F. Wu, *Corros. Sci.*, 80 (2014) 383.
20. O. A. Hazzazi, *J. Appl. Electrochem.*, 37 (2007) 933.
21. A. Pourghasemi Hanza, R. Naderi, E. Kowsari and M. Sayebani, *Corros. Sci.*, 107 (2016) 96.
22. A. M. El-Shamy, K.H. Zakaria, M. A. Abbas and S. Z. Abedin, *J. Mol. Liq.*, 211 (2015) 363.
23. B. Xu, Y. Ji, X. Zhang, X. Jin, W. Yang and Y. Chen, *J. Taiwan Inst. Chem. Eng.*, 59 (2016) 526.
24. S. Cao, D. Liu, H. Ding, K. Peng, L. Yang, H. Lu and J. Gui, *J. Mol. Liq.*, 220 (2016) 63.
25. M. Messali, A. Bousskri, A. Anejjar, R. Salghi and B. Hammouti, *Int. J. Electrochem. Sci.*, 10 (2015) 4532.
26. X. H. Li, S. D. Deng and H. Fu, *Int. J. Electrochem. Sci.*, 53 (2011) 1529.
27. Q. B. Zhang and Y. X. Hua, *Mater. Chem. Phys.*, 119 (2010) 57.
28. Y. Ma, F. Han, Z. Li and C. Xia, *ACS Sustainable Chem. Eng.*, 4 (2016) 5046.
29. N. A. Kermani, I. Petrushina, A. Nikiforov, J. O. Jensen and M. Rokni, *ACS Sustainable Chem. Eng.*, 41 (2016) 16688.
30. A. M. Atta, G. A. El-Mahdy, H. A. Allohedan and M. M. S. Abdullah, *Int. J. Electrochem. Sci.*, 11 (2016) 882.
31. H. Tian, W. Li and B. Hou, *Int. J. Electrochem. Sci.*, 8 (2013) 8513.
32. S.D. Deng, X.H. Li and X.G. Xie, *Corros. Sci.*, 80 (2014) 276.
33. X.H. Li, S.D. Deng, H. Fu and X.G. Xie, *Corros. Sci.*, 78 (2014) 29.
34. X. Zheng, S. Zhang, W. Li, M. Gong and L. Yin, *Corros. Sci.*, 95 (2015) 168.
35. Y. Qiang, L. Guo, S. Zhang, W. Li, S. Yu and J. Tan, *Sci. Rep.*, 6 (2016) 33305.
36. X. Ren, S. Xu and S. Chen, *RSC Adv.*, 5 (2015) 101693.
37. Y. Qiang, S. Zhang, S. Xu and L. Yin, *RSC Adv.*, 5 (2015) 63866.
38. Y. Qiang, S. Zhang, S. Xu and W. Li, *J. Colloid Interface Sci.*, 472 (2016) 52.
39. N. Chen, S. Zhang, Y. Qiang, S. Xu and X. Ren, *Int. J. Electrochem. Sci.*, 11 (2016) 7230.
40. A.O. Yüce, B.D. Mert, G. Kardas and B. Yazıcı, *Corros. Sci.*, 83 (2014) 310.
41. Ü. Ergun, D. Yüzer and K.C. Emregül, *Mater. Chem. Phys.*, 109 (2008) 492.
42. L. Guo, S. Zhu, S. Zhang, Q. He and W. Li, *Corros. Sci.*, 87 (2014) 366.
43. L. Luo, S. Zhang and Y. Qiang, *Int. J. Electrochem. Sci.*, 11 (2016) 8177.
44. M. Messali, A. Bousskri, A. Anejjar, R. Salghi and B. Hammouti, *Int. J. Electrochem. Sci.*, 10

(2015) 4532.

45. Y. Ma, F.Han, Z. Li and C. Xia, *ACS Sustainable Chem. Eng.*, 4 (2016) 5046.

46. Z. Wang , Y. Gong, C. Jing, H. Huang, H. Li, S. Zhang and F. Gao, *Corros. Sci.*, 113 (2016) 64.

47.M.A. Deyab, *J. Power Sources*, 292 (2015) 66.

48.H. S. M. Belayachi, A. El Assyry, H. Oudda, S. Boukhris and M. Ebn Touhami, *Int. J. Electrochem. Sci.*, 10 (2015) 3038.

49. A. Dutta, S. K. Saha, P. Banerjee and D. Sukul, *Corros. Sci.*, 98 (2015) 541.

© 2017 The Authors. Published by ESG (www.electrochemsci.org). This article is an open access article distributed under the terms and conditions of the Creative Commons Attribution license (<http://creativecommons.org/licenses/by/4.0/>).